frontiers | Frontiers in Earth Science

TYPE Original Research
PUBLISHED 19 September 2024
DOI 10.3389/feart.2024.1466751

OPEN ACCESS

EDITED BY
Haijun Qiu,
Northwest University, China

REVIEWED BY
Chang Zhou,
China University of Mining and Technology, China
Shuangshuang Wu,
Hohai University, China

*CORRESPONDENCE
Zhenwei Dai,
daizhenwei@mail.cgs.gov.cn

RECEIVED 18 July 2024
ACCEPTED 03 September 2024
PUBLISHED 19 September 2024

CITATION
Li Z, Dai Z, Cheng S, Yang Z, Zhang A and Xiong Q (2024) Study on the chain-type failure mechanism of large-scale ancient landslides.
Front. Earth Sci. 12:1466751.
doi: 10.3389/feart.2024.1466751

Study on the chain-type failure mechanism of large-scale ancient landslides

Zixuan Li[1,2], Zhenwei Dai [2]*, Shi Cheng[2,3], Zhe Yang[1,2], Anle Zhang[2,3] and Qihui Xiong[4]

[1]Institute of Geological Surve, China University of Geosciences, Wuhan, China, [2]Wuhan Center, China Geological Survey (Central South China Innovation Center for Geosciences), Wuhan, China, [3]College of Civil Engineering and Architecture, China Three Gorges University, Yichang, China, [4]Chongqing Bureau of Geology and Mineral Resources Exploration and Development Nanjiang Hydrogerlogy Engineering Geology Team, Chongqing, China

Large-scale ancient landslides are widely distributed in Southwest China, yet their reactivation mechanisms remain complex and poorly understood. On 25 July 2020, one such landslide in Liujing Village, Wulong District, Chongqing, China, experienced reactivation. This event exhibited variable movement characteristics across different areas and times, ultimately manifesting as a chain-type failure. Combining field investigations and drilling works, this study describes the fundamental characteristics of the Zhongbao landslide and the variation rules of the seepage field and the stability by numerical simulations. The failure mechanism is preliminarily revealed, and the failure influencing factors are discussed. The results show that, the landslide's progression was influenced by the stratigraphic lithology and the morphology of the sliding surface, resulting in two distinct turns during its movement. By analyzing the landslide's spatial morphology, direction of sliding, material composition, extent of the accumulation area, and dynamic behavior, we have categorized the Zhongbao landslide into five principal zones. The failure process can be segmented into four stages: initiation, shear-out, acceleration, and accumulation blockage. Heavy rainfall served as the primary trigger for the landslide, while the microtopography of the sliding surface significantly influenced the failure dynamics. The insights gained from this study offer valuable guidance for understanding the reactivation mechanisms of similar chained ancient landslides in the geologically analogous regions of Southwest China.

KEYWORDS

ancient landslide, failure mechanism, deformation characteristics, numerical analysis, GeoStudio

1 Introduction

Ancient landslides are landslides that have been inactive for a long time and the time of the last activity is not clear, usually consisting of mixed accumulations of complex genesis, dominated by lumpy soils, gravelly clasts, or pulverized clays interspersed with gravelly clasts, etc., with a disorganized and unstratified structure (Cruden and Varnes, 1996; Zhang et al., 2018). Ancient landslides are usually not easy to be recognized and are easily reactivated under the influence of rainfall infilt ration, artificial excavation, reservoir storage, etc., and are extremely destructive

due to their large amount of destabilized cubic meters (Georgi & Krastanov, 2015; Wartman et al., 2016). With the increase of human engineering activities and extreme climate in recent years, the resurgence of ancient landslides in southwest China has been increasing, further drawing attention to the study of ancient landslide deformation mechanisms (Guo et al., 2022). For example, the Leibo landslide in 2017 with a volume of 4.03 m^3 × 10^6 m^3, destroying under-construction roads and numerous buildings (He et al., 2019). The Jiangdingya landslide with a volume of 4.8–5.5 m^3 × 10^6 m^3, caused siltation of the river and buried toe villages and hydropower stations (Guo et al., 2019).

In-depth understanding of the reactivation mechanism of ancient landslides is crucial for implementing countermeasures and mitigating losses in engineering construction (Huang et al., 2021). A large number of studies have shown that the reactivation of ancient landslides is influenced by single or coupled factors such as geological formations, rainfall, reservoir level, and human activities, which lead to the deformation of landslides (Cheng et al., 2023; Dai et al., 2022; Qiu et al., 2024; Wei et al., 2024; Yang et al., 2023; Ye et al., 2024; Zhang et al., 2024).

Combined with centrifuge experiments, the deformation characteristics of the Cheyiping landslide were analyzed, which proved that even if the sliding surface is not deep, the sudden drop of the reservoir water level is the main controlling factor of the slope sliding. Zhang et al. (2020) conducted a preliminary analysis of the reactivation mechanism of Baiyangwan landslide through field investigation, drilling and on-site monitoring, and proved that the artificial slopes and valleys in mountainous areas may induce the elevation of groundwater level, and ultimately induce the reactivation of the landslide (Zhang et al., 2020). Tian et al. (2022) indicates that the formation of ancient landslides is closely related to the uplift of the Tibetan Plateau and the erosion of the Longwu River. Landslides characterized by zigzag sliding paths are relatively rare and present obvious directional changes, complicating risk assessment efforts (Tian et al., 2022). A case in point is the Niu'erwan landslide, which reactivated in 2020 and exhibited a sharp turn during its descent, resulting in two distinct mudslide zones. This event led to the destruction of eight houses, two critical roads, and extensive farmland damage (Zhou et al., 2022). The deformation and failure mechanisms of such ancient landslides remain inadequately understood, particularly the factors contributing to the development of these complex sliding patterns. Consequently, there is an urgent need for research to unravel these mechanisms and improve our predictive capabilities.

This study shows the fundamental features and deformation characteristics of the Zhongbao landslide, a prototypical large-scale ancient landslide characterized by zigzag patterns and a chain-type failure process. Combining field investigations, drilling, on-site shear tests, numerical analysis and laboratory shear tests, we conducted a preliminary analysis of its failure mechanism, specifically addressing the causes of its folded trajectory. Furthermore, we explored the significant influence of infiltration channels and rainfall on the landslide's reactivation. The findings of this research offer valuable insights into the reactivation mechanisms of ancient landslides under similar geological conditions in Southwest China, serving as a reference for future studies and risk management strategies.

2 Geologic setting

2.1 General description

Zhongbao landslide is located in Liujing Village, Wulong District, Chongqing, China. The region has complex topography, high mountains and deep valleys, and the overall terrain is high in the northeast and southwestern part of the country. The downward slope is mostly developed along the level of gray rock and shale, and the slope topography has a slope angle of 16°–55°, while the reverse slope is steep and localized as steep canyons. Landslide area near the deep cut along the Yanchang River, the formation of steep terrain, terrain height difference, coupled with long-term weathering, unloading effect, the formation of high steep slopes in the development of rock unloading Zone And fissure rock fragmentation zone, for the occurrence of landslides provide the conditions.

2.2 Climatic conditions

Landslide area belongs to the subtropical humid climate zone, warm and humid, abundant rainfall. The average temperature over the years is 18.1°. The average annual rainfall is 1191.8 mm, which indicating rainfall is abundant, However the time distribution is not uniform, the annual rainfall is mostly concentrated in April to September, with a rainfall of 846.9 mm, accounting for about 76% of the average annual rainfall. The study area is abundant with significant rainfall and karst water, whose combined effects significantly intensify the deformation and degradation of the slope's soft zones, fractured areas, and unloaded rock masses. Furthermore, the Canghe River's eroding action at the slope's base accentuates the steepness of the leading edge's topography. This geomorphological steepening furnishes propitious conditions conducive to the occurrence of landslide.

2.3 Geological formations

The landslide area is located in the southeastern edge of the Sichuan Basin, and the geotectonic structure is located in the Yangzi quasi-terraneous platform of Chongqing Taikai-o-Chongqing fold bundle of Wanzhou concave fold bundle range. The tectonic structure in the area is dominated by comb folds with a north-east-north-east orientation, and a series of pressure tectonic structures have been generated due to the extension of the Sichuan-Guizhou north-south radial tectonic belt, and a complex (S-shaped oblique connection) composite relationship is formed with the north-north-east-north-east tectonic structure, which makes the tectonic features more complicated. The regional tectonic system is characterized by the "blocking type" of geese rows arranged on the plane, and the fold axis is 15°–40°, and the axis is often in the shape of "S." Dorsal slope is narrow, narrow strip, two asymmetric wings, generally steep south east wing, north west wing slow; to the slope is wide and slow, two wings nearly symmetrical, stratigraphic dip angle 10°–30°. Based on the field investigation, the stratigraphic yield of the landslide is 135°–142°∠17°–26°.

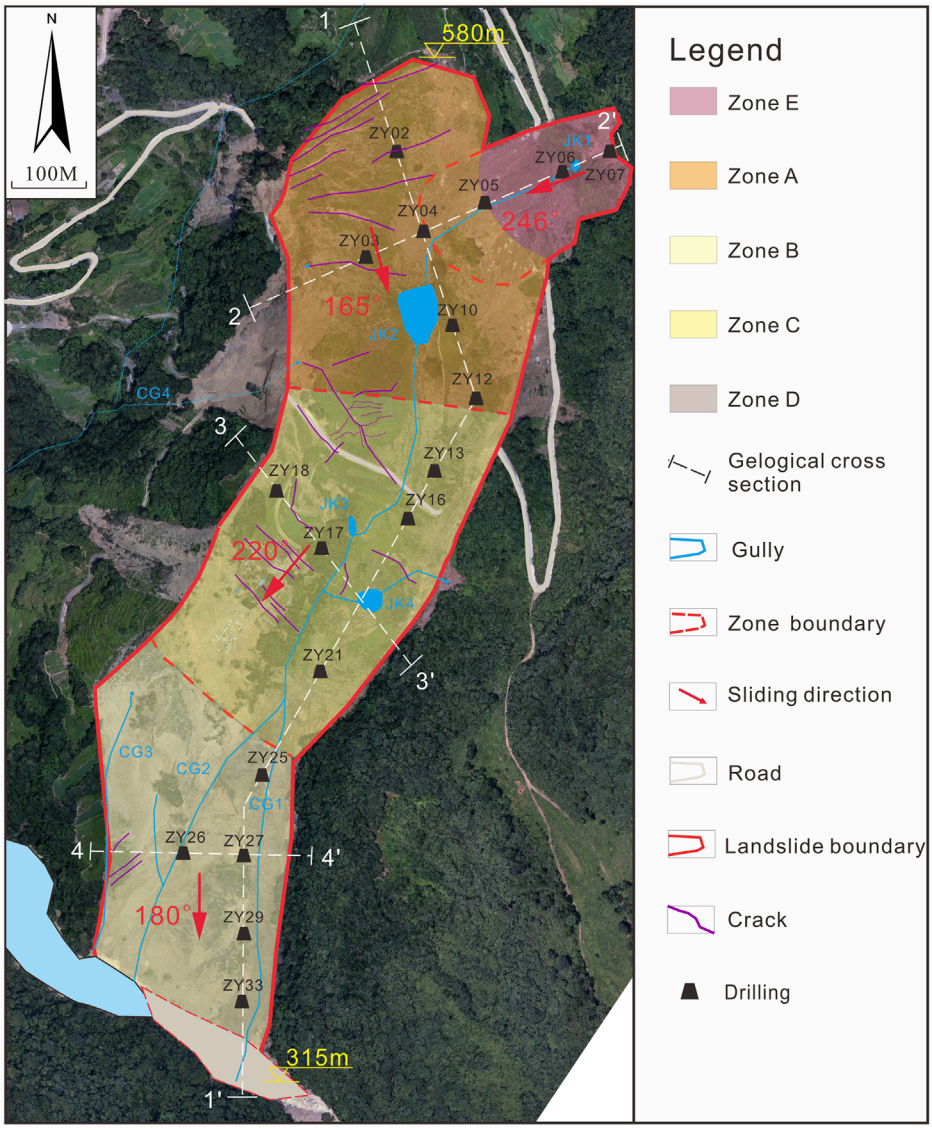

FIGURE 1
Plan view of the Zhongbao landslide. The landslide is divided into five subzones, which are the trailing edge nudging Zone A, extrusion and turning Zone B, leading edge tangential accumulation and stacking Zone C, weir counterpressure Zone D, and trailing edge soil slip Zone E.

3 Characteristics of landslides

3.1 Landslide characteristics

The overall plan form of Zhongbao landslide is in the shape of a "long tongue." There were two turns in sliding process, the main slip direction of 150°–220°, basically along the north-south direction of the spread (Figure 1). The longitudinal length is about 850 m, transverse width is about 200 m, thickness is about 3.5–66.2 m, volume is about 5.48 $m^3 \times 10^6$ m^3, which is a large rock-soil landslide. The slope angle of the rear edge of the landslide is 5°–12°, the slope angle of the middle edge is 8°–17°, and the slope angle of the front edge of the landslide is 25°–45°, with a general trend of steepness at the front edge and slowness at the rear edge (Figure 2). The volume of the landslide that collapsed into the river was about 54 $m^3 \times 10^3$ m^3, the width of the blocked river section was about 25–40 m, and the length of the blocked river was about 150 m.

3.2 Hydrogeolofical conditions

After the sliding of the Zhongbao landslide, four catchment pits JK1-JK4, four gullies CG1-CG4, and eight springs were formed in the landslide body (Figure 1). CG1 and CG2 have intermittent water flow in the gullies in the normal times, and are basically connected during the rainy season, while CG3 and CG4 do not have any water flow during normal times, and the water flow in the gullies intermittently exists in the rainy season, and is occasionally discharged downstream along with the mudslides. Directly converge into the downstream Yancang River, and CG4 converges with the seasonal washout on the outside of

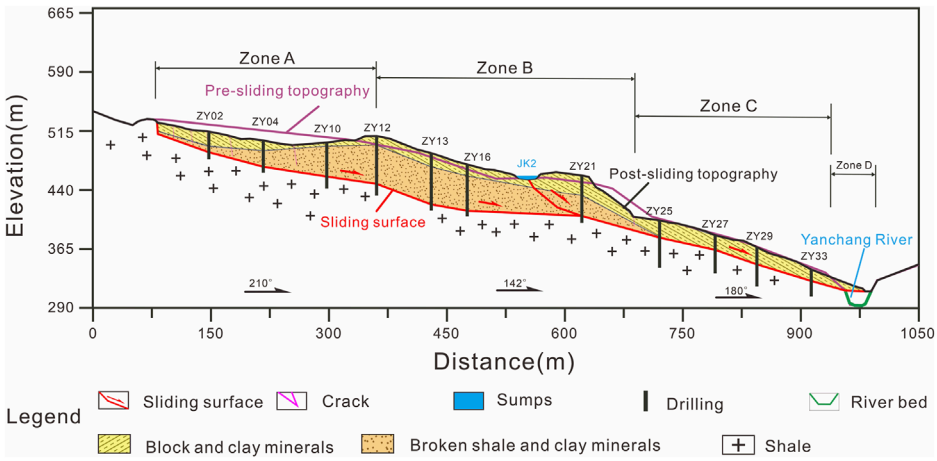

FIGURE 2
Geological section 1-1′ in Figure 3.

the landslide area to flow into the downstream Yancang River. Based on the simple hydrological observation in the field, the non-rainy season flow of CG1 and CG2 is about 0.05–0.3 m^3/s, and the rainy season flow is about 0.3–0.7 m^3/s; the rainy season flow of CG3 and CG4 is about 0.1–0.6 m^3/s.

Test pit seepage experiments were conducted in 20 boreholes in the study area and pumping experiments were carried out in boreholes ZY3, ZY18 and ZY27. The permeability coefficients of 4.33×10^{-5}~1.01×10^{-2} cm/s for the massive rock sandwiched powdery clay were obtained, which were dominated by weakly permeable-moderately permeable layers, and some strongly permeable layers existed at the back edge of the landslide; the permeability coefficients of 9.52×10^{-5}~6.30×10^{-3} cm/s for the fragmented rock body were obtained, which were dominated by weakly permeable-moderately permeable layers. Groundwater in the landslide area can be divided into loose rock pore water, bedrock fissure water and karst water according to the characteristics of water-bearing medium and storage state. Groundwater recharge in the study area mainly consists of atmospheric rainfall and karst water, and groundwater is generally rich.

3.3 Material composition

The material composition and structural characteristics of the Zhongbao landslide were revealed through detailed field investigations and drilling. In order to obtain the mechanical properties of the soil samples, *in situ* shear experiments and laboratory shear experiments were carried out to determine the shear strength and internal friction angle of the soil samples obtained from the sliding body and sliding surface (Table 1).

Sliding body: the sliding body is mainly composed of Quaternary Holocene avalanche deposits (Q_4^{col+dl}) and paleo-landslide accumulations (Q_4^{del}). There is a large difference between the trailing and leading edge of the landslide slide bodies. The trailing edge slide varies greatly in the vertical direction, with the upper part mainly consisting of massive rocky soil sandwiched with clay (Q_4^{col+dl}), which is about 3.5–18.4 m thick; the lower part mainly consists of fragments of rocky body sandwiched with clay (Q_4^{del}), which becomes thicker and thinner from north to south and west to east, with a general thickness of 20.0–66.2 m. The fore-edge slide is mainly consisting of massive rocky soil sandwiched with clay (Q_4^{col+dl}) with a similar character to that in the upper part of the trailing edge (Figure 2).

Sliding bed: the sliding bed mainly consists of greenish gray shale ($S_{2h\text{-}Sh}$) of Hanjiadian Formation in the middle part of the Liou system, with muddy structure, thin laminations, developed shale, the main mineral composition is clay minerals, and the fissures are more developed. Drilling holes ZY24, ZY25, ZY26, and ZY31 indicate that there are localized muddy and weak interlayers in the lower part of the rock body in Area C, but there is no sign of sliding.

Sliding zone:The sliding zone primarily consists of the ancient landslide accumulation layer (Q_4^{del}), characterized by gray-green and light yellow clayey soils interspersed with gravel. The zone is subject to intense pressure, resulting in predominantly light yellow and dark gray clayey soils with a high plasticity particle content ranging from 60% to 80%. These soils are notably sticky to the touch and exhibit a pronounced sludging effect, softening rapidly upon contact with water. Borehole investigations reveal that the sliding zone typically has a thickness ranging from 0.2 to 1.5 m, while exploratory wells expose a soil thickness of approximately 0.4 m within the sliding zone. The interface with the underlying hard rock stratum shows distinct signs of abrasion, and in places, a polished, mirror-like surface is observable (Figure 4C). Notably, the sliding zone's thickness at the rear edge of Area A is less than that at the central front, and the depth and thickness of the sliding zone on the eastern side exceed those on the western side.

4 Landslide reactivation deformation characteristics

According to the boreholes, the upper part of the landslide body in A and B areas is a loose structure of lumpy soil, and the lower part of the landslide body is a fragmented rock body and soil body with dense cementation and chaotic rock body

TABLE 1 Engineering geologic zoning.

Landslide subdivision	Length (m)	Width (m)	Average thickness (m)	Volume (10^6 m^3)	Slip angle (°)	Gradient (°)
Zone A	280	180	35	1.76	165	20
Zone B	300	170	25	2.55	220	9–11
Zone C1	220	60	50	0.05	180	18
Zone C2	290	80	4	0.35	180	21
Zone E	150	180	15	0.72	250	30–50
Volume of Zone D (10^6 m^3)	$54\ m^3 \times 10^3\ m^3$					
Volume of the landslide (10^6 m^3)	$5.48\ m^3 \times 10^6\ m^3$					

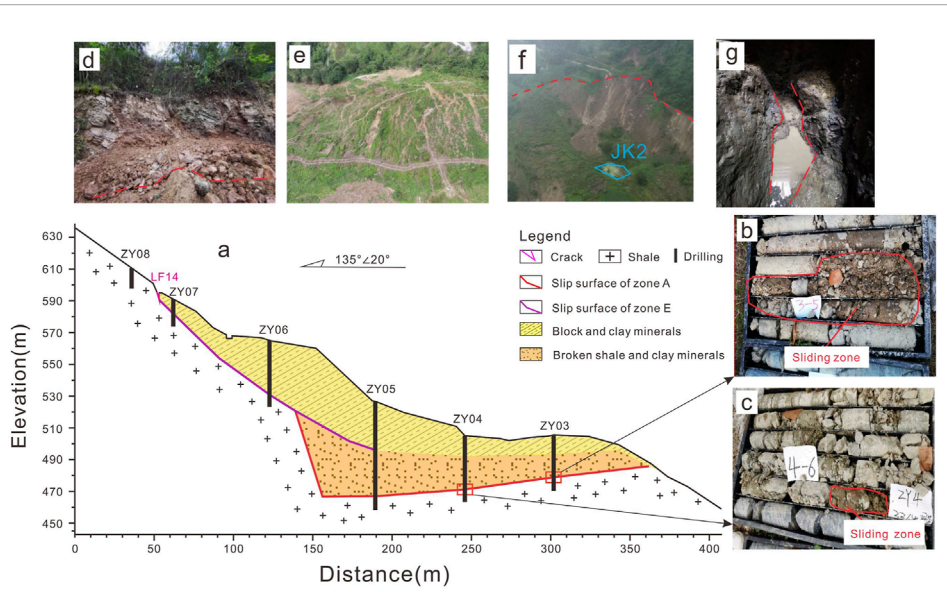

FIGURE 3
Cross-section of Area **(A)**. The sliding direction is towards the inside of the papera. **(A)** 2–2′ section **(B)** ZY3 slip zone, depth 24.4 m–27.0 m **(C)** ZY4 slip zone, depth 33.5 m–34.0 m **(D)** Folding of crushed rock after extrusion **(E)** West of the junction of Areas A and B, large number of plume fissures formed in the surface soil after extrusion **(F)** East of the junction of Areas A and B, catchment pit JK2 **(G)** TJ1 exposing tensile fracture faulting.

layer sequence. The Zhongbao landslide has obvious characteristics of ancient landslide accumulation body, so it is speculated that the Zhongbao landslide is an ancient landslide reactivation. The sliding direction of Zhongbao landslide has been turned twice at a large angle, and the overall direction of movement is in the form of a folding line. The deformation characteristics of different areas of Zhongbao landslide have obvious differences, the overall failure has obvious stages, and the reactivation deformation process has chain characteristics. According to the deformation history of the landslide, combined with the material composition and structural characteristics of the landslide, the landslide is divided into five subzones (Figure 1), which are the trailing edge nudging Zone A, extrusion and turning Zone B, leading edge tangential accumulation and stacking Zone C, weir counterpressure Zone D, and trailing edge soil slip Zone E. Their characteristics are shown in Table 1.

4.1 Zone A

Since 18 July 2020, a large number of surface cracks and tensile faults appeared in the surface layer of Area A. Detailed field investigations revealed its macrodeformation characteristics. A large number of feather-like cracks after extrusion can be seen in the upper surface layer on the west side of the junction location of Area A and Area B (Figure 3E), and the exposed rock body can be seen to be folded after extrusion of the fractured rock body (Figure 3D), and the results of the trenching indicate that the fractured rock

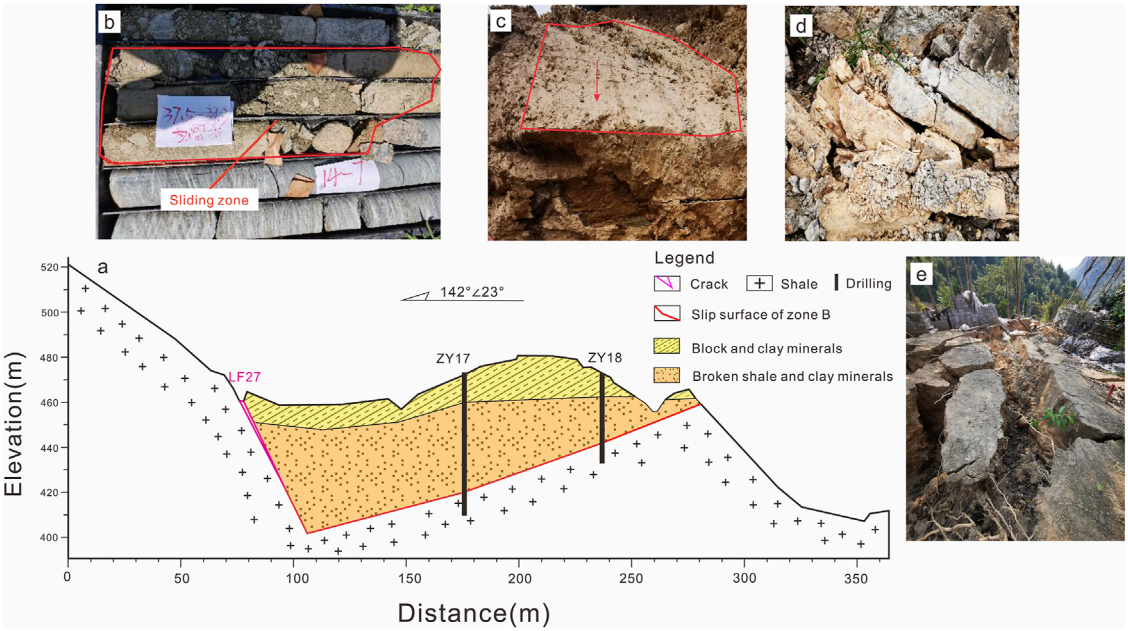

FIGURE 4
Section of Zone **(B)**. The sliding direction is towards the inside of the paper. **(A)** 3–3′ section **(B)** Core sample from sliding fracture zone **(C)** Smooth mirror friction marks **(D)** Front edge of Zone B pushing out cluttered rock mass **(E)** Fracture in central Zone B.

body in the lower part of Area A undergoes pulling and cracking wrongcanning, and the seams are developed (Figure 3G). According to the drilling, the eastern slide body is more fragmented than the central and western slide bodies, and the fractured rock body has messy stratigraphy.

4.2 Zone B

On 22 July 2020, Zone B began to slide slowly, with a sliding direction of 220°, forming pullout slots on both sides that continued to expand and also caused destruction of roads and cracking of building surfaces (Figure 4E). Drill hole 17 reveals that the slip zone in area B is mainly dominated by clay sandwiched with rubble blocks, and the rubble blocks are extruded and milled strongly, and part of them are rounded and arranged in a directional manner (Figure 4B). The back edge of area C can see that the sheared rock body of area B has been wrongly fractured, and part of the rock body can be seen to have a mirror-like abrasion (Figures 4C, D). The area B is sheared at the back edge of area C2, and the sheared rock body of the broken rock body has produced bending and bulging reversal, and the rock layer has been wrongly fractured.

4.3 Zone E

The sliding of the fractured rock body in Zone A of the trailing edge push resulted in the lower part of the soil body on the east side being adjacent to the air, and the upper part of the thick layer of soil body and sliding downward along the bedrock surface with a direction of 250° to form Zone E. The sliding of Zone E covered the upper part of Zone A, which increased the self-weight of Zone A. The *in situ* infiltration testing showed that a moderately permeable layer was formed in the middle and rear part of the slide body. The *in situ* infiltration testing showed that a moderately permeable layer was formed in the middle and rear part of the slip body, and a low permeability layer was formed locally. Surface water and groundwater from the trailing edge continued to pour in, forming catchment pit JK2 at the junction of zones A and B, with a water depth of about 2–5 m.

4.4 Zone C and Zone D

The Zone C can be subdivided into two subsections, C1 and C2, based on its deformation characteristics. On 24 July 2020, noticeable deformation commenced in the Zone C2,while multiple fissures emerged at the forefront of the Zone C1, accompanied by a series of clicking noises reminiscent of thunder that persisted over time. Although the shallow slide masses in the zones C1 and C2 partially entered the river, they did not create a barrier dam. With the leading edge becoming unstable and the trailing edge subjected to additional loading, the landslide as a whole experienced an accelerated downward movement, particularly in the AB area where a marked increase in velocity was observed. Concurrently, the landslide's sliding direction underwent another alteration, shifting from 220° to 180°.

On 25 July 2020, rainfall occurred in the landslide zone, at which time Zone C1 began to slide, Zone C2 slid twice, traces of secondary sliding were visible on the exposed landslide wall (Figure 5B), and the sliding body entered the river along the Cang River to form a weir. At the same time, due to rainfall, the surface rock and soil bodies in Zone C formed a debris flow and slid downward, accelerating the expansion of the weir, blocking the river length of about 150 m and depth of about 12 m.

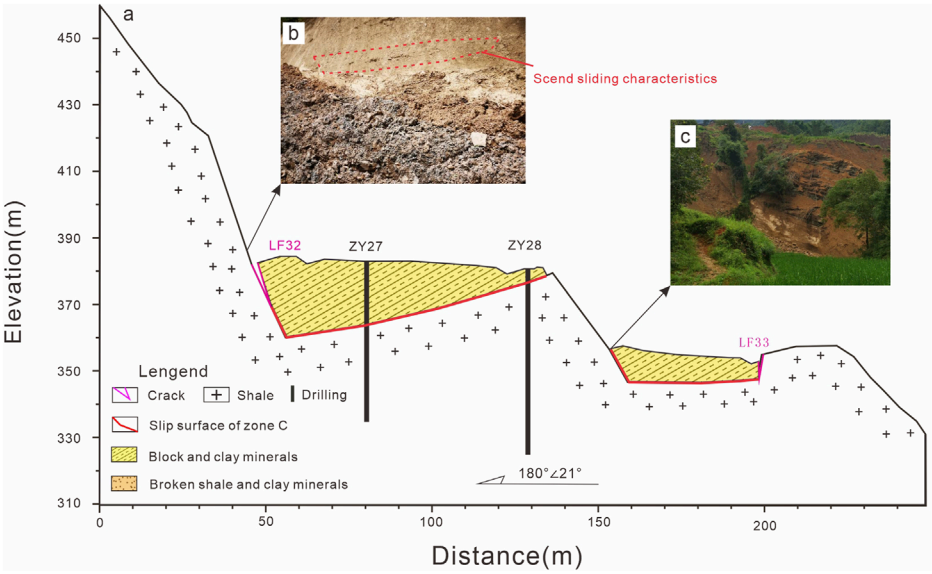

FIGURE 5
Cross section of zones C1 and C2. The sliding direction is towards the inside of the paper **(A)** 4–4′ profile **(B)** Secondary slide marks in Zone C2 **(C)** Eastern rubbing of Zone C1.

5 Numerical analysis of the landslide

5.1 Calculation model of the landslide

The numerical model (Figure 6) for seepage and FOS analysis was established using the GeoStudio software and the computational domain of the model was discretized into a mixture of triangular and quadrilateral elements, with a total of 17,472 nodes and 17,528 elements. Based on the numerical model of the Zhongbao Landslide (Figure 6), the SLOPE/W module was used to analyse the stability of the landslide under rainfall fluctuation by coupling the transient seepage field distribution data of the landslide obtained by the SEEP/W module at different time periods. The Morgenstern-Price limit equilibrium method in the SLOPE/W module was used to systematically analyse the variation of the stability of the zhongbao Landslide as rainfall changed for a duration of 20 days. The main physico-mechanical parameters used in the numerical analysis were selected based on the laboratory test results of the rock and soil mass of the landslide. Then, the values of the parameters used in the numerical model were finally determined by comparing the *in situ* measured groundwater and surface deformation data of the landslide with the results of the numerical inversion, as listed in Table 2.

5.2 Results

5.2.1 Seepage field simulation results

The relationship curve of pore water pressure with rainfall time at three typical monitoring points at the contact surface between the slip surface and bedrock is shown in Figure 7. There are obvious differences in the time to reach saturation across different areas (Figure 7). And the front reaches saturation first, followed by the middle and rear, which is presumed to be related to the thickness and the material. Under the action of groundwater and rainfall, the pore water pressure at point A is always higher than that at points B and C, which leads to the effective stress near point A is always in a lower state, which also cause the rear edge of the landslide to be the first to appear cracks and begin to slip.

5.2.2 Investigation of the variation of landslide stability with time

In the initial stage of rainfall, the FOS of the landslide is about 1.07, which is in a stable state; after that, with the continuous infiltration of rainfall the stability of the landslide decreases; after the extreme rainfall on July 15, the rate of decrease of the stability of the landslide increases until the stability of the landslide on July 22 falls to 0.99, which is in an unstable state. After that,the rate of decrease of the stability decreases continuously and stabilizes at 0.98 nearby (Figure 8). This result is consistent with the deformation of the landslide. In this process, continuous rainfall caused the pore water pressure of the sliding zone increased rapidly, the sliding mass transitioned from the saturated state to the supersaturated state and coupled with the influence of seepage formed by rainfall, the stability of the landslide greatly reduced.

6 Discussion

6.1 Predisposing factors and trigger

6.1.1 Geomorphology

The average slope angles of the three parts of the Zhongbao landslide slide surface from top to bottom, Zone A, Zone B, and Zone C, are about 20°, 10°, and 19°, respectively, while the slope

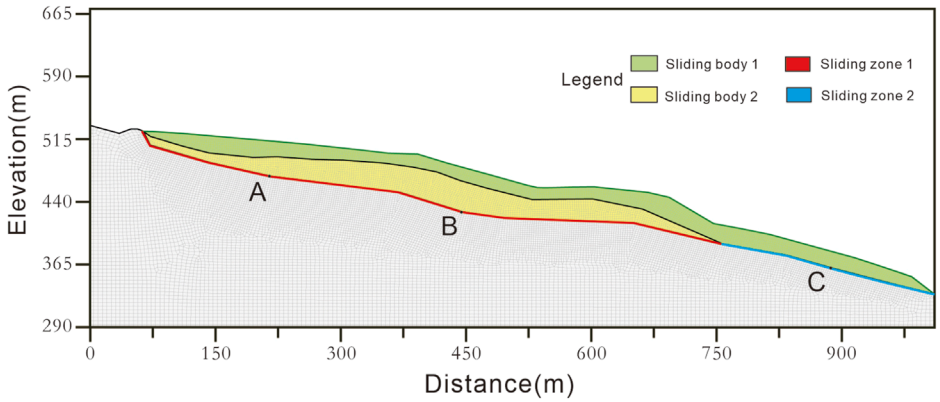

FIGURE 6
Finite element model of the Zhongbao landslide.

TABLE 2 The shear strength parameters of the materials.

	Moisture content (%)	Unit weight (kN/m^3)	Cohesive (kPa)	Internal friction angle (°)
Sliding body 1 (Q_4^{col+dl})	28.50	21.3	22.6	14.3
Sliding body 2 (Q_4^{del})	29.20	24.2	15.6	36.3
Sliding zone 1 Zone A&B	29.50	27.6	21.9	11.3
Sliding zone 2 Zone C	25.70	27.5	29.4	16.9

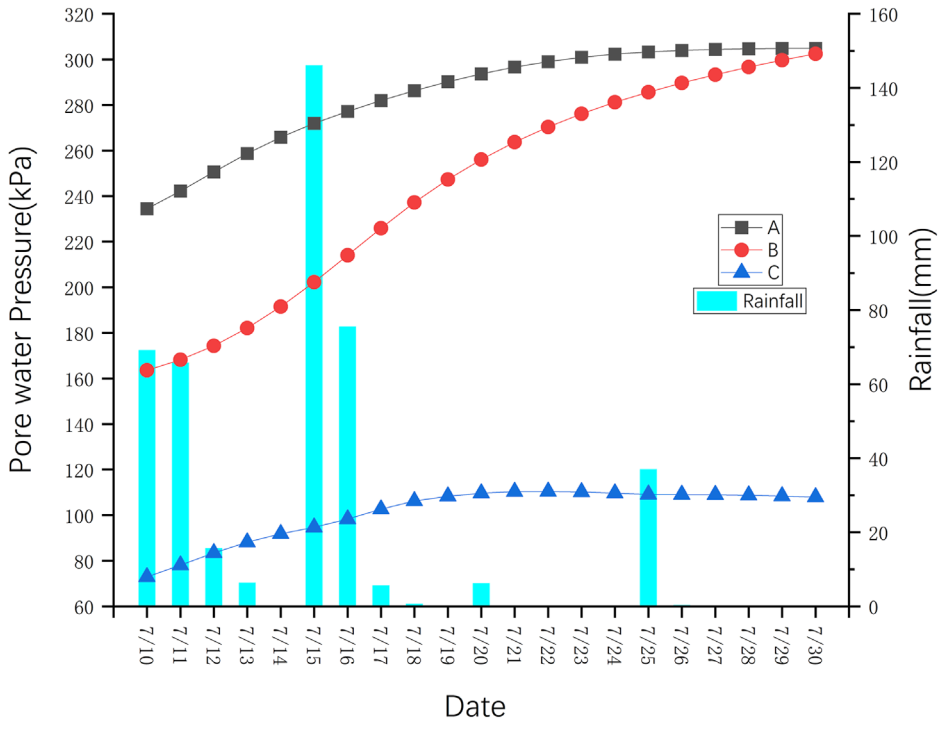

FIGURE 7
Relationship curves between pore pressure and rainfall time of typical monitoring points.

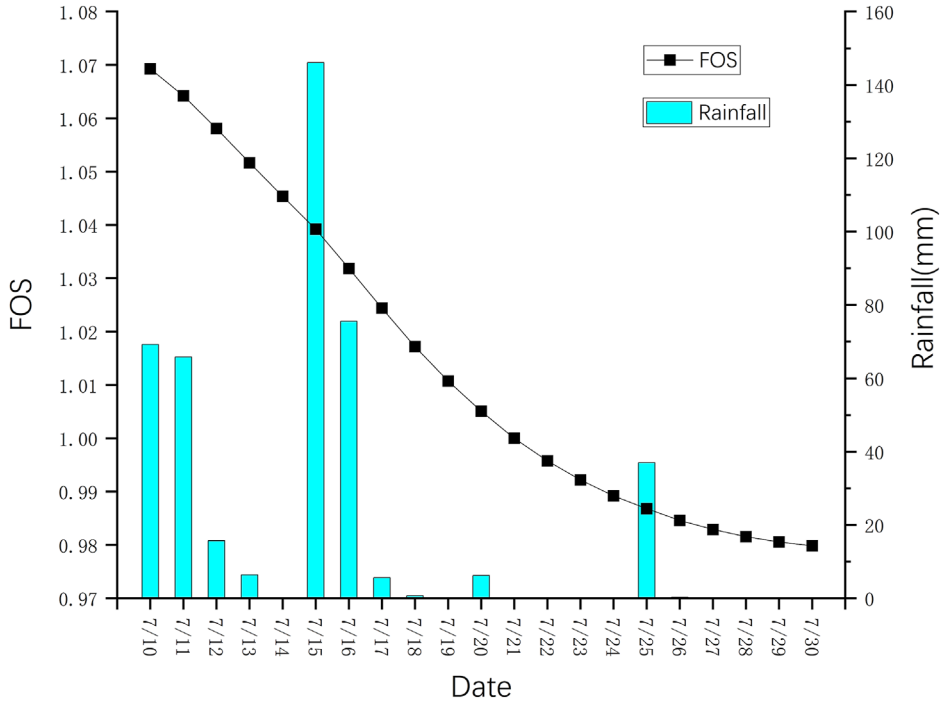

FIGURE 8
Relationship between safety factor and rainfall time.

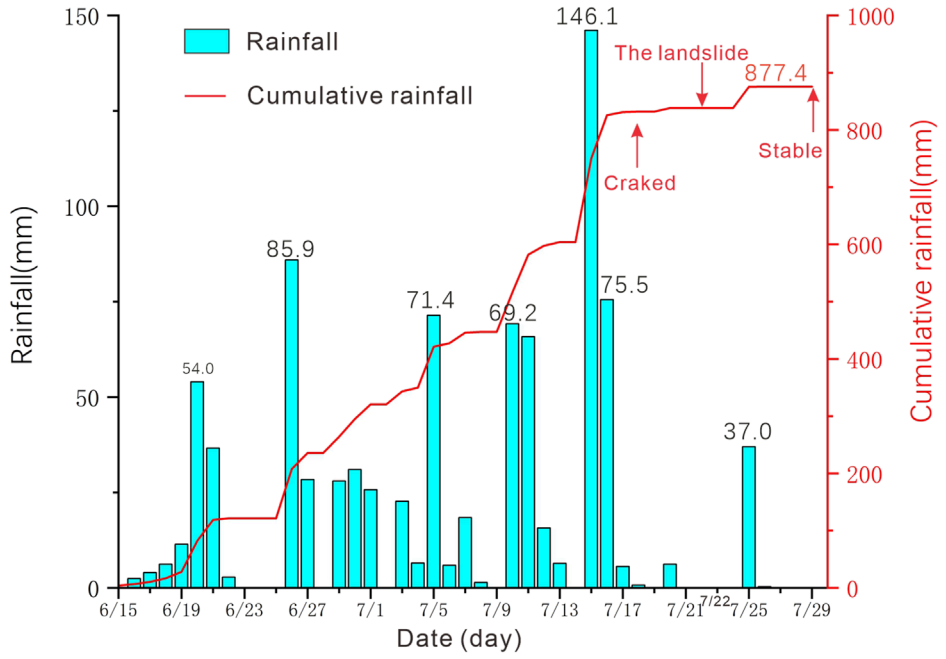

FIGURE 9
Rainfall monitoring data from Tongzi rainfall station which is 8.3 km far from Zhongbao landslide.

angle of Zone E is as high as 30~50°. The steep slope source zones in the upper part, Zone A and Zone E, provide activation conditions for landslide failure. The central part is gentle and provides a platform for landslide potential energy accumulation. The steep and narrow foot of the slope provides a channel for the landslide to enter the river (Zhou et al., 2022).

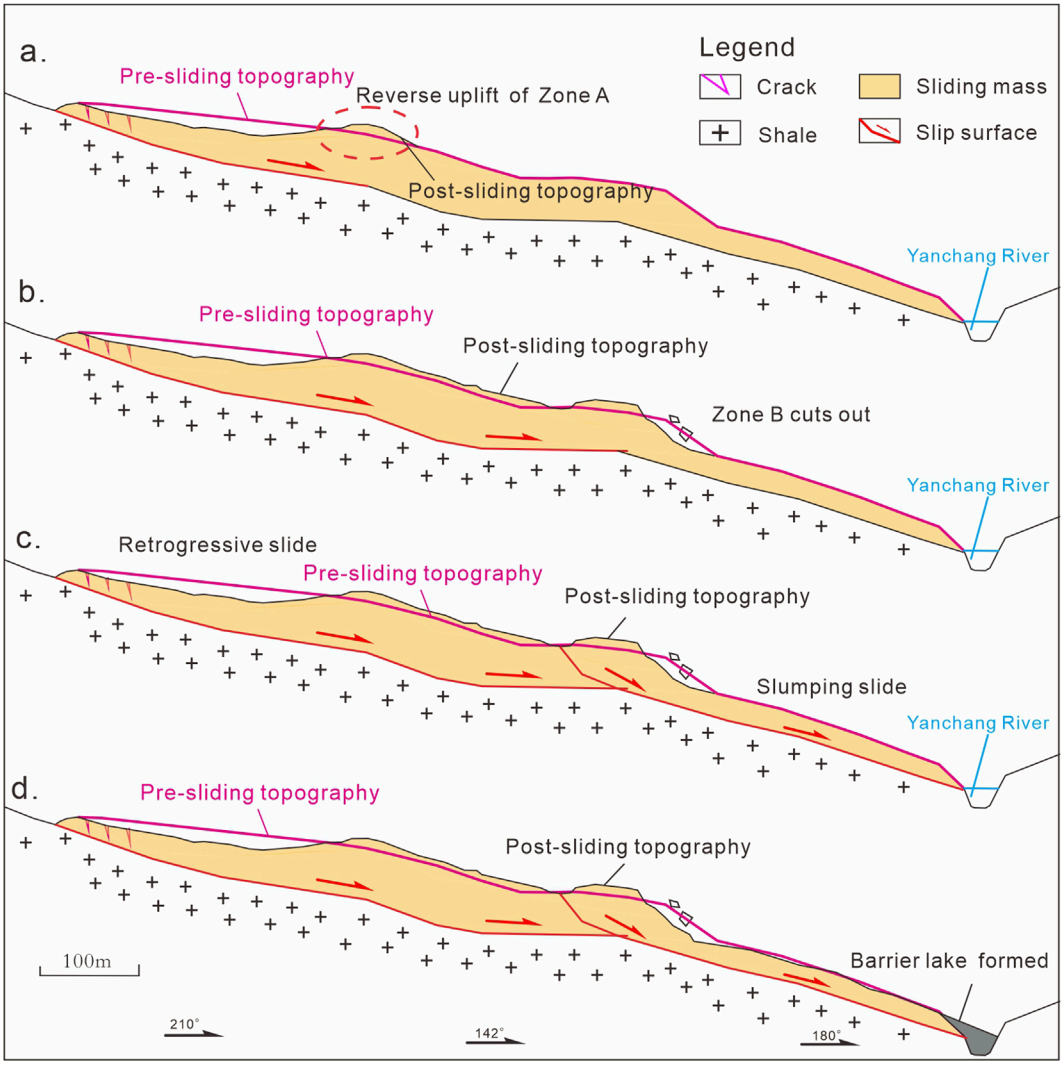

FIGURE 10
Characteristic diagram of instability. **(A)** Initiation phase. **(B)** Shearing out stage. **(C)** Acceleration phase. **(D)** Accumulation and blockage stage.

6.1.2 Persistent rainfall

Sustained rainfall as a trigger for landslides (Huang et al., 2022; Peruccacci et al., 2017; Senthilkumar et al., 2018; Wu and Yeh, 2020). There were several high-intensity rainfalls in the month prior to the failure of the Zhongbao landslide, with a cumulative rainfall of 227.2 mm in the first 3 days, and a cumulative rainfall during the slip period amounted to 43.6 mm (Figure 9). The continuous rainfall pooled through the surface into the middle and rear depressions of the landslide to allow the surface water to infiltrate downward, which would saturate the soft Zone Between bedrock surfaces with water, which would not only reduce the shear strength of the soft layer, but also soften the soils in the location of the interface of the soft layer, contributing to the reactivation of its landslide. Meanwhile, the presence of a moderately permeable layer at the trailing edge of the landslide keeps the shear strength of the soil body at a low level, creating favorable conditions for landslide slippage.

6.2 Possible failure mechanism

The occurrence of the Zhongbao landslide is the result of the combined effect of geological factors and rainfall factors. Based on the results of field site investigations, *in situ* experiments and laboratory experiments, combined with the deformation history of the Zhongbao landslide, its failure process is divided into four stages.

1. Initiation phase (Figure 10A). Under the action of rainfall and groundwater, multiple cracks appeared in Zone A, and then the landslide began to slide slowly. According to the surface deformation characteristics of Zone A combined with the characteristics of the borehole slip surface, it is hypothesized that the landslide body in the process of sliding, due to the east side of the ridge of the blocking constraints, resulting in the sliding of the fractured rock body biased to the west to produce steering, resulting in the lower part of the rock body

by the extrusion of some of the fractured rock body level of the inverted warping phenomenon. As a result, the slip direction of the landslide turned from 165° to 220°.

2. Shearing out stage (Figure 10B). Driven by Zone A, Zone B also started to slide slowly. Zone B sheared out at the upper edge of Zone C2, and part of the slide body flowed into Zone C2. The outcrop is broken and misaligned. Combined with the borehole results, it is hypothesized that Zone B was similarly blocked by the east side of the rock mass during the movement. Under the impetus of Zone B, sliding began to occur in Zone C2. At the junction of Zone B and Zone C, the sliding direction changed from 220° to 180°, and the angle of the sliding surface changed from 20° to 10°, which increased the anti-sliding force and the stability of the landslide.
3. Acceleration phase (Figure 10C). After the rainfall on the 25th, the deformation of the landslide was obviously accelerated. Sliding occurred in the upper part of Zone E, which was piled up on top of Zone A, increasing the deadweight of the slide; secondary deformation occurred in Zone C2, as evidenced by the traces of secondary sliding on the wall of the landslide (Figure 6B). The first two stages of sliding accumulated potential energy in the central platform, but due to the increase of the self-weight of the trailing edge and the sliding of the leading edge, the potential energy accumulated by the landslide began to be released, and the overall performance was accelerated sliding, which led to the sliding of the residential zone in Zone B by about 90 m.
4. Accumulation and blockage stage (Figure 10D). The landslide continued to move, and Zone C entered the river to form a weir, blocking the river and threatening the safety of residents along the downstream. Meanwhile, under the effect of rainfall and gravity, mudslides occurred in Zone C, gradually expanding the volume of the weir. It continued until 30 July 2020, when the sliding gradually stopped.

In summary, the Zhongbao landslide, as indicated by its deformation history and drilling results, is a large-scale rocky-soil landslide. Its reactivation is primarily driven by a combination of back-edge pushing and front-edge loosening. The inadequate drainage of the underlying bedrock prevented timely discharge of infiltrated rainwater, leading to a consequent reduction in shear strength of the sliding zone in zones A and B. During its movement, the landslide exhibited a sliding motion along the slip surface, characterized by the extrusion of soft clay against hard bedrock, which macroscopically manifested as a directional turn. The turning behavior of the Zhongbao landslide is influenced by both the stratigraphic lithology and the topography of the slip surface. A thorough understanding of the mechanisms behind such multi-directional steering landslides can enhance early warning systems for landslides in similar geological settings and contribute valuable insights into their deformation mechanisms.

7 Conclusion

This paper focuses on the Zhongbao landslide, conducting a comprehensive study through detailed field geological surveys, engineering geological investigations, and laboratory tests to elucidate its failure mechanism. The conclusions are as follows:

1. The Zhongbao landslide predominantly distributes elevations between 295–600 m. Its overall morphology resembles an elongated "tongue," having undergone multiple slides with two principal changes in direction. The main slip orientation ranges from 150 to 220°, extending approximately 850 m in length and 200 m in width, with a thickness varying from 3.5 to 66.20 m and an estimated volume of 5.48×10^6 cubic meters. This classifies it as a large-scale rocky-soil landslide.
2. According to the spatial morphology of the landslide, slip turn direction, material composition, accumulation Zone Combined with the movement process of the Middleburg landslide, the landslide was divided into five major zones respectively, namely, trailing edge push shift Zone A, extrusion turn Zone B, leading edge tangential accumulation and stacking Zone C, weir counterpressure Zone D, and trailing edge soil slip Zone E. The landslide was divided into five major zones, namely, trailing edge thrust Zone A, squeeze turn Zone B, leading edge tangential stacking and stacking Zone C, weir counterpressure Zone D, and trailing edge soil slide Zone E.
3. Prolonged rainfall facilitated the reactivation of the original ancient slide surface, leading to the formation of a continuous slip surface. Infiltration of surface water and groundwater into the bedrock's soft surface, which is structurally very loose, along with the persistent weakening effect of groundwater, has progressively reduced the shear strength of the weak surface, resulting in downward deformation of the landslide.
4. The Zhongbao landslide, characterized by a back-edge push, a loosened front edge, and a complete reactivation of the original ancient landslide accumulation, has impacted roads, houses, and navigation channels. The landslide's movement, influenced by the geotechnical properties and the slip surface morphology, underwent two directional shifts and formed a weir. This study provides insights for early warning and risk assessment of landslides in similar geological environments.

Data availability statement

The original contributions presented in the study are included in the article/supplementary material, further inquiries can be directed to the corresponding author.

Author contributions

ZL: Data curation, Methodology, Software, Writing–original draft, Writing–review and editing. ZD: Funding acquisition, Investigation, Methodology, Project administration, Writing–original draft, Writing–review and editing. SC: Writing–original draft, Writing–review and editing. ZY: Writing–original draft, Writing–review and editing. AZ: Data curation, Formal Analysis,

Software, Writing–original draft, Writing–review and editing. QX: Resources, Writing–original draft, Writing–review and editing.

Funding

The author(s) declare that financial support was received for the research, authorship, and/or publication of this article. The work was supported by a follow-up of the Geological Disaster Prevention and Control Project in the Three Gorges area (Grant No. 000121 2023C C60 001 and Grant No. 000121 2021C C60 001), Qianlong Plan Top Talent Project of Wuhan Center of China Geological Survey (Grant No. QL2022-06).

Acknowledgments

The authors would like to thank Chongqing Bureau of Geology and Mineral Resources Exploration and Development Nanjiang Hydrogerlogy Engineering Geology Team,for the great assitance in field investigation and providing date.

Conflict of interest

The authors declare that the research was conducted in the absence of any commercial or financial relationships that could be construed as a potential conflict of interest.

Publisher's note

All claims expressed in this article are solely those of the authors and do not necessarily represent those of their affiliated organizations, or those of the publisher, the editors and the reviewers. Any product that may be evaluated in this article, or claim that may be made by its manufacturer, is not guaranteed or endorsed by the publisher.

References

Cheng, Z., Liu, S., Fan, X., Shi, A., and Yin, K. (2023). Deformation behavior and triggering mechanism of the Tuandigou landslide around the reservoir area of Baihetan hydropower station. *Landslides* 20 (8), 1679–1689. doi:10.1007/s10346-023-02093-9

Cruden, D. M., and Varnes, D. J. (1996). Landslide types and processes, special report, transportation research board. *U.S. Natl. Acad. Sci.* 247, 236–275.

Dai, Z., Zhang, Y., Zhang, C., Luo, J., and Yao, W. (2022). Interpreting the influence of reservoir water level fluctuation on the seepage and stability of an ancient landslide in the three Gorges reservoir area: a case study of the outang landslide. *Geotechnical Geol. Eng.* 40 (9), 4551–4561. doi:10.1007/s10706-022-02170-1

Georgi, F., and Krastanov, M. (2015). "Evaluation of the possibilities for construction on ancient landslide," in Engineering Geology for Society and Territory, Springer, Cham, 04 January 2015 (Springer), 267–271. doi:10.1007/978-3-319-09057-3_39

Guo, C., Zhang, Y., Li, X., Ren, S., Yang, Z., Wu, R., et al. (2019). Reactivation of giant jiangdingya ancient landslide in zhouqu county, gansu province, China. *Landslides* 17 (1), 179–190. doi:10.1007/s10346-019-01266-9

Guo, C., Zhang, Y., Yuan, H., Liu, D., Yan, Y., Hua, S., et al. (2022). Study of an ancient landslide reactivation mechanism based on centrifuge model testing: an example of the Jiangdingya ancient landslide reactivation in 2018, Gansu Province, China. *Landslides* 20 (1), 127–141. doi:10.1007/s10346-022-01978-5

He, K., Ma, G., Hu, X., Luo, G., Mei, X., Liu, B., et al. (2019). Characteristics and mechanisms of coupled road and rainfall-induced landslide in Sichuan China. *Geomatics, Nat. Hazards Risk* 10 (1), 2313–2329. doi:10.1080/19475705.2019.1694230

Huang, F., Chen, J., Liu, W., Huang, J., Hong, H., and Chen, W. (2022). Regional rainfall-induced landslide hazard warning based on landslide susceptibility mapping and a critical rainfall threshold. *Geomorphology* 408, 108236. doi:10.1016/j.geomorph.2022.108236

Huang, X., Wang, L., Ye, R., Yi, W., Huang, H., Guo, F., et al. (2021). Study on deformation characteristics and mechanism of reactivated ancient landslides induced by engineering excavation and rainfall in Three Gorges Reservoir area. *Nat. Hazards* 110 (3), 1621–1647. doi:10.1007/s11069-021-05005-z

Peruccacci, S., Brunetti, M. T., Gariano, S. L., Melillo, M., Rossi, M., and Guzzetti, F. (2017). Rainfall thresholds for possible landslide occurrence in Italy. *Geomorphology* 290, 39–57. doi:10.1016/j.geomorph.2017.03.031

Qiu, H., Su, L., Tang, B., Yang, D., Ullah, M., Zhu, Y., et al. (2024). The effect of location and geometric properties of landslides caused by rainstorms and earthquakes. *Earth Surf. Process. Landforms* 49 (7), 2067–2079. doi:10.1002/esp.5816

Senthilkumar, V., Chandrasekaran, S. S., and Maji, V. B. (2018). Rainfall-Induced landslides: case study of the marappalam landslide, nilgiris District, Tamil nadu, India. *Int. J. Geomechanics* 18 (9). doi:10.1061/(asce)gm.1943-5622.0001218

Tian, J.-j., Li, T.-t., Pei, X.-j., Ding, F., Sun, H., Xie, X.-g., et al. (2022). Formation and reactivation mechanisms of large-scale ancient landslides in the Longwu River basin in the northeast Tibetan Plateau, China. *J. Mt. Sci.* 19 (6), 1558–1575. doi:10.1007/s11629-021-7261-x

Wartman, J., Montgomery, D. R., Anderson, S. A., Keaton, J. R., Benoît, J., dela Chapelle, J., et al. (2016). The 22 march 2014 oso landslide, Washington, USA. *Geomorphology* 253, 275–288. doi:10.1016/j.geomorph.2015.10.022

Wei, Y., Qiu, H., Liu, Z., Huangfu, W., Zhu, Y., Liu, Y., et al. (2024). Refined and dynamic susceptibility assessment of landslides using InSAR and machine learning models. *Geosci. Front.* 15 (6), 101890. doi:10.1016/j.gsf.2024.101890

Wu, C.-Y., and Yeh, Y.-C. (2020). A landslide probability model based on a long-term landslide inventory and rainfall factors. *Water* 12 (4), 937. doi:10.3390/w12040937

Yang, X., Jiang, Y., Zhu, J., Ding, B., and Zhang, W. (2023). Deformation characteristics and failure mechanism of the moli landslide in guoye town, zhouqu county. *Landslides* 20 (4), 789–800. doi:10.1007/s10346-022-02019-x

Ye, B., Qiu, H., Tang, B., Liu, Y., Liu, Z., Jiang, X., et al. (2024). Creep deformation monitoring of landslides in a reservoir area. *J. Hydrology* 632, 130905. doi:10.1016/j.jhydrol.2024.130905

Zhang, C., Yin, Y., Dai, Z., Huang, B., Zhang, Z., Jiang, X., et al. (2020). Reactivation mechanism of a large-scale ancient landslide. *Landslides* 18 (1), 397–407. doi:10.1007/s10346-020-01538-9

Zhang, Q., Jia, C., Chen, H., Zheng, Y., and Cheng, W. (2024). Centrifuge modeling test on reactivation of ancient landslide under sudden drop of reservoir water and rainfall. *Acta Geotech.* 19, 5651–5672. doi:10.1007/s11440-023-02217-4

Zhang, Y., Wu, R., Guo, c., Wang, l., Yao, x., and Yang, z. (2018). Research progress and prospect on reactivation of ancient landslides. *Advans Earth Sci.* in Chinese. 33 (7), 728–740. doi:10.11867/j.issn.1001-8166.2018.07.0728

Zhou, C., Huang, W., Ai, D., Xu, H., Yuan, J., Kou, L., et al. (2022). Catastrophic landslide triggered by extreme rainfall in Chongqing, China: July 13, 2020, Niuerwan landslide. *Landslides* 19 (10), 2397–2407. doi:10.1007/s10346-022-01911-w